A Probabilistic Approach to Series Arc Fault Detection and Identification in DC Microgrids

Kaushik Gajula[®], *Member, IEEE*, Vu Le[®], *Member, IEEE*, Xiu Yao[®], *Senior Member, IEEE*, Shaofeng Zou[®], *Member, IEEE*, and Luis Herrera[®], *Member, IEEE*

Abstract—In this article, series arc fault detection and identification is investigated for dc microgrids using a statistical model based on nodal analysis. The consecutive sample difference of the injection currents are modeled as a random vector whose distribution depends on the network conductance matrix. When a series fault occurs, the conductance matrix changes, which leads to a change in the data generating distribution. The goal is to quickly detect and identify faults on different lines while maintaining low false alarm rates. A quickest change detection (QCD) approach is proposed in this article, utilizing a cumulative sum (CUSUM) algorithm. The proposed method is robust to nominal network operations, such as load and reference changes, and the CUSUM statistic is used for detection increase during faults, ensuring faults are not missed. In addition, a Kron reduction approach is developed to eliminate the internal nodes, and an optimal sensor placement strategy is proposed using vertex cover to ensure fault detection on any line with reduced number of sensors. The proposed framework is tested on dc microgrids typically found in the more electric aircraft, composed of multiple generators, internal nodes, and various load types. Lastly, experimental results are shown on a microgrid testbed to validate the feasibility of the QCD approach for series arc fault detection.

Index Terms—Constant current load (CCL), constant power load (CPL), cumulative sum (CUSUM) algorithm, dc microgrids, fault detection and identification, Kullback-Leibler (KL) divergence, quickest change detection (QCD).

I. INTRODUCTION

C SERIES arc faults present a significant challenge for the reliable operation of dc microgrids. These faults occur when a current is transmitted through a plasma channel in series with the circuit, often as a result of a wire break or tear [1]. The resulting arc discharge creates a high-impedance plasma that resembles a resistor in series with the circuit, leading to low-fault current levels that can be difficult to detect using traditional protection methods [2], [3], [4]. Furthermore, the noise generated by the series arc fault can propagate through the

Manuscript received 9 January 2023; revised 18 April 2023, 6 July 2023, and 28 September 2023; accepted 29 October 2023. Date of publication 8 November 2023; date of current version 5 January 2024. This work was supported by the National Science Foundation under Grant 1855888, Grant 1948165, and Grant 1809839. (Corresponding author: Luis Herrera.)

The authors are with the Department of Electrical Engineering, University at Buffalo, Amherst, NY 14068 USA (e-mail: kaushikk@buffalo.edu; vule@buffalo.edu; xiuyao@buffalo.edu; szou3@buffalo.edu; lcherrer@buffalo.edu;

Color versions of one or more figures in this article are available at $\frac{1}{100}$ https://doi.org/10.1109/JESTIE.2023.3331183.

Digital Object Identifier 10.1109/JESTIE.2023.3331183

network and potentially be misdetected by independent current sensors [4], [5].

Detection strategies for series dc arc faults have primarily focused on analyzing and extracting features of the line current during a fault event. The noise generated by the plasma channel serves as a key factor in detecting these faults. Time domain strategies for identifying series arc faults involve examining the statistical properties of the line current to determine the presence of an arc fault. For instance, Abdullah et al. [6] analyzed the line current to detect the presence of added noise by calculating the Hurst exponent of the signal, a measure of its randomness. Similarly, the authors in [7] and [8] proposed methods for detecting the presence of (pink) noise generated by the dc series arc fault [3], [9]. Other time domain-based methods include the computation of the sample entropy [10], recurrence methods for characterizing the determinism of the signal [11], and autoregressive moving average estimation [12]. Frequency and time-frequency domain methods have also gained traction due to their ability to quickly detect higher frequency changes in the line current caused by a series arc fault. These include several approaches including wavelet transform [4], [13], [14] and Fourier transform [15], [16].

The existing literature offers various examples of features that can be used to detect series arc faults within a single line. This allows for the natural development of machine learning methods that combine multiple features to optimize detection strategies [17]. For instance, the authors in [18] and [19] presented an ensemble machine learning approach that combines several classification techniques, such as support vector machine, k-nearest neighbor, and random forest, to create an optimal detection strategy. Neural networks have also been employed for series arc fault detection in studies, such as [20], [21], [22], and [23]. Deep learning methods, including long short-term memory and gated recurrent learning, have been explored for dc series arc fault detection in [24], [25], and [26]. Finally, random forest strategies have gained popularity as machine learning methods for series arc fault detection in research, such as [27] and [28]. However, these methods focus on the detection of series arc fault in a single line.

Although numerous detection techniques for series arc faults exist, several challenges and drawbacks remain. For instance, detecting a series arc fault and pinpointing the faulted line is a complex problem that requires a large number of sensors [29], [30], [31], [32], [33]. Moreover, mistriggers can occur in adjacent lines, as the noise from series arc faults can propagate within

2687-9735 © 2023 IEEE. Personal use is permitted, but republication/redistribution requires IEEE permission. See https://www.ieee.org/publications/rights/index.html for more information.

the network [5], [31]. Centralized techniques, such as time-based parameter estimation algorithms, require nodal voltage and injection current measurements [32] or their estimates [33] at all nodes of a dc microgrid. Furthermore, machine learning techniques demand a substantial amount of training data, which may be challenging or cumbersome to obtain from existing systems.

This article presents a methodology for detecting and identifying series arc faults in dc microgrids. A statistical model of the network is developed to represent both normal and faulted conditions. The problem of detecting changes in the distribution of measurements from normal to faulted is formulated using the quickest change detection (QCD) framework [34], [35], [36], [37]. Specifically, QCD involves observing a stochastic system sequentially and detecting changes in the data generating distribution as quickly as possible (minimizing worst case detection delay), subject to false alarm constraints. The QCD approach has been applied for solving various problems in power systems, e.g., anomaly and line outage detection and identification in power networks [38], [39], [40], [41], [42], [43], fault detection in photovoltaic systems [44], voltage quality monitoring [45], cyber-attack detection in smart grid [46], [47], [48], and preliminary work in series arc fault detection [49]. See [37] for a review of recent studies using the QCD method in power systems. The main contributions of this article are as follows.

- A statistical model for general dc microgrids is developed using nodal analysis and the impact of series arc fault to the current measurement vector distribution is derived.
- 2) The series arc fault detection and line identification problem is formulated as a QCD problem, where it is assumed that at some unknown time a series arc fault occurs, which changes the probability distribution of the measured currents. The cumulative sum (CUSUM) algorithm is then used to solve the QCD problem and detect/identify the faulted line.
- 3) A Kron reduction technique is proposed for networks with internal nodes, and a vertex cover technique is also developed to reduce the number of sensors needed for accurate series are fault detection and identification.

Lastly, simulation and experimental results are shown to validate the implementation feasibility of the proposed approach.

The rest of this article is organized as follows. In Section II, a statistical model for the dc microgrid during normal and faulted conditions is derived. In Section III, the QCD-based fault detection method is presented. Simulation results are presented in Section IV with different case studies, and experimental results are provided in Section V. Finally, Section VI concludes this article.

The following notation is used in this article. Given a set \mathcal{X} , its cardinality is denoted by $|\mathcal{X}|$. The symbols 1_m and 0_n denote column vectors of m ones and n zeros, respectively. An $n \times n$ identity matrix is written as \mathcal{I}_n . The Kullback–Leibler (KL) divergence measures the difference between two probability distributions $f_{(m,n)}(x)$ and $f_0(x)$, where $f_0(x)$ is the reference distribution. The KL divergence is defined as

$$D(f_{(m,n)}||f_0) \triangleq \int f_{(m,n)}(x) \log \frac{f_{(m,n)}(x)}{f_0(x)} dx.$$
 (1)

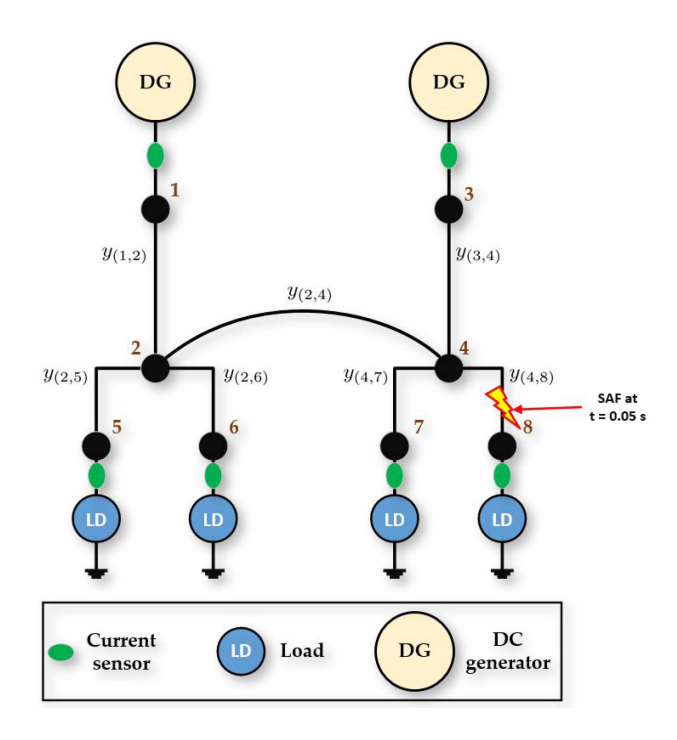


Fig. 1. Distribution system of a more electric aircraft [51], [52], [53], [54].

II. STATISTICAL MODEL FOR DC MICROGRID

A dc microgrid can be represented by a directed graph $\mathcal{G}=(\mathcal{V},\mathcal{E})$ [50], where \mathcal{V} is the set of nodes/buses and \mathcal{E} is the set of edges/lines (i,j) such that $i,j\in\mathcal{V}$. The number of nodes in the microgrid is given by $N=|\mathcal{V}|$. The neighborhood set of a node i in \mathcal{G} is denoted by $\mathfrak{N}_{\mathcal{G}}(i)$, which includes all the adjacent nodes that are incident to node i. The conductance of the line (m,n) is defined by $y_{(m,n)}$, while the line resistance is denoted by $y_{(m,n)}=\frac{1}{y_{(m,n)}}$. During steady state, a dc microgrid is governed by the following nodal equations:

$$I[k] = YV[k] \tag{2}$$

where $I[k] \in \mathbb{R}^N$ is a vector of injection currents, $Y \in \mathbb{R}^{N \times N}$ is the conductance matrix, $V[k] \in \mathbb{R}^N$ is a vector of bus voltages, and k represents the sampling instant. In Fig. 1, a typical dc distribution system used in a more electric aircraft is shown [51], [52], [53], [54]. In this case, the microgrid is defined as $\mathcal{G} = (\mathcal{V}, \mathcal{E})$, where the set of nodes are $\mathcal{V} = \{1, 2, \ldots, 8\}$ and the set of edges/lines are $\mathcal{E} = \{(1, 2), (2, 4), (3, 4), (2, 5), (2, 6), (4, 7), (4, 8)\}$. Therefore, there are N = 8 nodes and $|\mathcal{E}| = 7$ edges.

A. DC Microgrid Probabilistic Model

We begin by defining the difference between consecutive samples of the injection current vector $I[k] \in \mathbb{R}^N$ and nodal voltage vector $V[k] \in \mathbb{R}^N$ as

$$\Delta I[k] = I[k] - I[k-1] \tag{3}$$

$$\Delta V[k] = V[k] - V[k-1].$$
 (4)

Equation (2) can then be written as

$$\Delta I[k] = Y \Delta V[k]. \tag{5}$$

During normal operation, the voltage difference vector, $\Delta V[k] \in \mathbb{R}^N$ is assumed to be an independent identically distributed (i.i.d.) multivariate Gaussian random variable described as follows:

$$\Delta V[k] \sim \mathcal{N}(0_N, \Upsilon)$$
 (6)

where $\Delta V[k]$ has a mean of 0_N and the covariance as $\Upsilon = E[\Delta V[k]\Delta V[k]^T] \in \mathbb{R}^{N\times N}$. This assumption stems from the presence of power electronics at each node in the network (source or load), which establish a well-defined voltage source. The noise of these voltage sources can be modeled as Gaussian random variables [55], [56], [57], [58]. In Section III-C, we consider the case with internal nodes, i.e., no source or load converters.

Using (5), the covariance of the measured current difference vector, $\Delta I[k]$, can be obtained as follows:

$$E\left[\Delta I[k]\Delta I[k]^T\right] = E\left[Y\Delta V[k]\left(Y\Delta V[k]\right)^T\right]$$
$$= YE\left[\Delta V[k]\Delta V[k]^T\right]Y^T \tag{7}$$

$$\Rightarrow E\left[\Delta I[k]\Delta I[k]^T\right] = \Sigma_0 = Y \Upsilon Y^T. \tag{8}$$

The mean of $\Delta I[k]$ can similarly be derived as

$$E[\Delta I] = E[Y\Delta V] = YE[\Delta V] = 0. \tag{9}$$

Therefore, the current difference satisfies

$$\Delta I[k] \sim \mathcal{N}(0_N, \ \Sigma_0) \tag{10}$$

where the covariance $\Sigma_0 \in \mathbb{R}^{N \times N}$ is defined as $\Sigma_0 = Y \Upsilon Y^T$. We denote the normal or prefault Gaussian probability distribution function (pdf) of $\Delta I[k]$ as [59]

$$f_0\left(\Delta I[k]\right) = \frac{\exp\left(-\frac{1}{2}(\Delta I[k])^T \Sigma_0^{-1}(\Delta I[k])\right)}{\sqrt{(2\pi)^N \det(\Sigma_0)}}.$$
 (11)

B. Series Arc Fault-Based Model

A series arc fault can be modeled in a steady state as an increase in line resistance, due to a break in the line, which can be caused by wear and tear or loosely connected wires [4]. Fig. 2 shows a typical series arc fault model on a single line (m,n) [60], [61]. This model is composed of two elements: the additional arc fault resistance, $r_{(m,n)f}$, and $V_{\rm arc}$, which is used to model the noise caused by the plasma channel in [61] (Thevenin equivalent), and voltage drop in [60]. In this article, we utilize $V_{\rm arc}$ primarily as a source of noise injection [3], [9], [61].

After a series arc fault occurs on line (m, n), the line conductance decreases (line resistance increases) as shown below:

$$y_{(m,n)\gamma} = \frac{1}{r_{(m,n)} + r_{(m,n)f}}$$
(12)

where $r_{(m,n)}$ is the line resistance, $r_{(m,n)f}$ is the fault resistance, and γ is the change point, i.e., the instant of time when the series arc fault occurs. In addition to the change in line resistance, a series arc fault is also characterized by the introduction of fault noise $V_{\rm arc}$, which affects adjacent sensors in the network. This

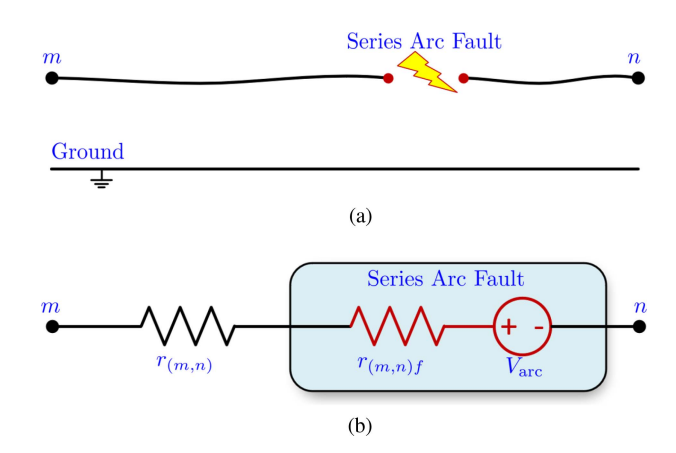


Fig. 2. Circuit view and model of a series arc fault. (a) Series arc fault in line (m, n). The break in the line and arc fault occurs in series. (b) Electrical series arc fault model on line (m, n).

voltage source can be assumed to be as follows:

$$V_{\text{arc}} \sim \mathcal{N}(\mu_{V_{\text{arc}}}, \psi)$$
 (13)

where $V_{\rm arc} \in \mathbb{R}$ is assumed to be independent of $\Delta V[k]$. The mean and variance of $V_{\rm arc}$ are $\mu_{V_{\rm arc}}$ and $\psi>0$, respectively. See [3], [9], and [61] for more details on the noise characteristics of dc series arc faults. In particular, the mean value of the arc voltage, $\mu_{V_{\rm arc}}$, can be modeled by a nonlinear function of the gap distance, which is generally slow varying compared with the time steps of the algorithm. For this reason, its difference between consecutive samples can be estimated as

$$\Delta V_{\rm arc}[k] \sim \mathcal{N}(0, \ \psi).$$
 (14)

Considering Fig. 2(b), the voltage drop across line (m, n) during a series arc fault satisfies

$$V_m - V_{\text{arc}} - V_n = I_{mn} \left[r_{(m,n)} + r_{(m,n)f} \right]$$
 (15)

where I_{mn} is the current flowing from node m to n. Using (12) and (15), the line current is derived as

$$I_{mn} = y_{(m,n)\gamma} [V_m - V_n] - y_{(m,n)\gamma} [V_{arc}].$$
 (16)

The nodal equation at node m is then given by

$$I_{m} = -y_{(m,n)\gamma} \left[V_{\text{arc}} \right] + \sum_{i \in \mathfrak{N}_{\mathcal{G}}(m)} y_{(m,i)} \left[V_{m} - V_{i} \right]$$
 (17)

while at node n we have

$$I_n = y_{(m,n)\gamma} [V_{\text{arc}}] + \sum_{i \in \mathfrak{N}_{\mathcal{G}}(n)} y_{(n,i)} [V_n - V_i].$$
 (18)

By using the above equations we define the matrix $Y_{(m,n)} \in \mathbb{R}^{N \times N}$, associated with a series arc fault on line (m,n), where the variable $y_{(m,n)}$ is replaced by $y_{(m,n)\gamma}$. The fault free model in (5) for ΔI is then changed during a series arc fault in line (m,n) to

$$\Delta I[k] = Y_{(m,n)} \Delta V[k] + B_{(m,n)} \Delta V_{\text{arc}}$$
 (19)

where $B_{(m,n)} \in \mathbb{R}^N$ is a column vector of zeros, except with $-y_{(m,n)\gamma}$ and $y_{(m,n)\gamma}$ at mth and nth node's indices, respectively.

The arc voltage, $V_{\rm arc}$, and the difference in nodal voltage, ΔV , are assumed to be independent since the series arc fault's discharge along the line (m,n) is primarily dependent on the mean of the line current [4]. Using this assumption, the covariance of ΔI in a postfault scenario is then calculated as

$$E\left[\Delta I[k]\Delta I[k]^{T}\right] = E\left[Y_{(m,n)}\Delta V[k]\left(Y_{(m,n)}\Delta V[k]\right)^{T}\right] + E\left[B_{(m,n)}\Delta V_{arc}\left(B_{(m,n)}\Delta V_{arc}\right)^{T}\right]$$
(20)

$$E\left[\Delta I[k]\Delta I[k]^{T}\right] = Y_{(m,n)}E\left[\Delta V[k]\Delta V[k]^{T}\right]Y_{(m,n)}^{T} + B_{(m,n)}E\left[\Delta V_{\text{arc}}\Delta V_{arc}^{T}\right]B_{(m,n)}^{T}$$
(21)

$$E\left[\Delta I[k]\Delta I[k]^{T}\right] = Y_{(m,n)} \Upsilon Y_{(m,n)}^{T} + B_{(m,n)} \psi B_{(m,n)}^{T}$$
(22)

$$\Rightarrow \Sigma_{(m,n)}$$

$$= Y_{(m,n)} \Upsilon Y_{(m,n)}^{T} + B_{(m,n)} \psi B_{(m,n)}^{T}$$
(23)

and the mean of ΔI is derived as

$$E[\Delta I] = Y_{(m,n)}E[\Delta V] + B_{(m,n)}E[\Delta V_{\text{arc}}] = 0 \qquad (24)$$

since $E[\Delta V] = 0$ and $E[\Delta V_{arc}] = 0$.

The difference in current during a fault on line (m, n) is then modeled using a different distribution

$$\Delta I[k] \sim \mathcal{N}(0_N, \ \Sigma_{(m,n)})$$
 (25)

where the covariance $\Sigma_{(m,n)} \in \mathbb{R}^{N \times N}$ is defined as $\Sigma_{(m,n)} = Y_{(m,n)} \Upsilon Y_{(m,n)}^T + \psi B_{(m,n)} B_{(m,n)}^T$. The postfault pdf of $\Delta I[k]$ for a series arc fault in line $(m, n) \in \mathcal{E}$ is then denoted as

$$f_{(m,n)}(\Delta I[k]) = \frac{\exp\left(-\frac{1}{2}(\Delta I[k])^T \Sigma_{(m,n)}^{-1}(\Delta I[k])\right)}{\sqrt{(2\pi)^N \det(\Sigma_{(m,n)})}}.$$
 (26)

C. Voltage Covariance Estimation

In this article, we assume the nodal voltage difference covariance matrix, $\Upsilon = E[\Delta V[k]\Delta V[k]^T]$, to be unknown. Therefore, it needs to be estimated using measurements from voltage sensors at all nodes. This can be accomplished either from historical data or be updated at a slower time rate. For example, collecting a set of P samples of $\Delta V \in \mathbb{R}^N$, we can then compute the following empirical covariance matrix Γ :

$$\Gamma = \operatorname{cov}\left(\Delta V[1] \quad \cdots \quad \Delta V[P]\right).$$
 (27)

This process can be done in an iterative manner to keep track of any variations/disturbances in ΔV . We further improve the empirical estimate using the following:

$$\hat{\Upsilon} = q\Gamma + R \tag{28}$$

where R is a diagonal matrix and q is a positive scalar. In this case, the matrix R is used to increase the impact of the variance of each local node voltage.

D. Time Step Selection

The statistical models used in this article for normal, (5), and fault, (19), conditions assume a static representation of the network behavior using nodal analysis. This is an accurate description for small dc microgrids where the line inductance is negligible (e.g., nano Henry range). However, for larger dc microgrids, the line inductance can affect the behavior of the line currents, which can more accurately be modeled by a dynamic system of the form

$$\frac{dI_{ij}}{dt} = -\frac{r_{(i,j)}}{L_{(i,j)}}I_{ij} + \frac{1}{L_{(i,j)}}(V_i - V_j) \quad \text{or} \quad (29)$$

$$I_{ij}[k+1] = e^{-\frac{1}{\tau_{(i,j)}}T_{QCD}}I_{ij}[k]$$

$$+ \frac{1}{r_{(i,j)}} \left(1 - e^{-\frac{1}{\tau_{(i,j)}} T_{\text{QCD}}} \right) \left(V_i[k] - V_j[k] \right)$$
 (30)

where $(i,j) \in \mathcal{E}$ is a line, $\tau_{(i,j)} = \frac{L_{(i,j)}}{r_{(i,j)}}$ is the time constant, T_{QCD} is the algorithm time step, and (30) is derived using the zero-order hold. Therefore, for larger line inductances, the algorithm time step should be chosen to be approximately equal to the largest line time constant, i.e., $T_{\text{QCD}} \approx \max_{(i,j) \in \mathcal{E}} \tau_{(i,j)}$. This recommendation is based on the convergence of (30) to the static nodal analysis case as the time step increases (modeling errors are decreased) and the inherent robustness to model errors of the proposed QCD algorithm [62].

III. QUICKEST FAULT DETECTION AND IDENTIFICATION

In this section, we present the CUSUM algorithm for solving the quickest fault detection and identification problem [34]. We also analyze the series arc fault detection with full and partial current sensors.

A. Full Information

Let τ be a stopping time, i.e., the instant of time series arc fault is detected/identified, and γ be the change point or instant the series arc fault occurs. The objective of QCD is to minimize the average detection delay subject to false alarm constraints. This problem can be formulated as

$$\min_{\tau} \sup_{\gamma > 0} E_{\gamma} \left[\tau - \gamma \mid \tau \ge \gamma \right]$$
 subject to $E_{\infty} \left[\tau \right] \ge \beta$ (31)

where β is a positive scalar constraint on the mean time to false alarm [63], E_{γ} denotes the expectation when the fault happens at time γ , and E_{∞} denotes the expectation when there is no fault.

The CUSUM algorithm [34] is then adopted to solve the above QCD problem due to its recursive computation and optimality properties [34]. For a fault at line (m, n), it utilizes the normal and postfault pdfs, f_0 and $f_{(m,n)}$, shown in (11) and (26), respectively. The CUSUM algorithm, then, computes the following statistic for each line, $(m, n) \in \mathcal{E}$, in the network:

$$W_{(m,n)}[k+1]$$

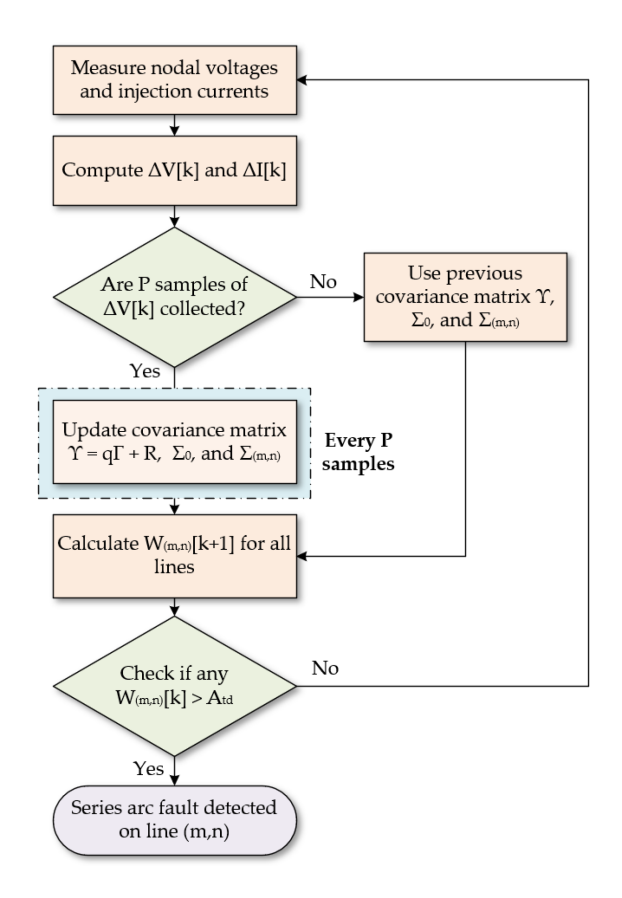


Fig. 3. CUSUM algorithm for series arc fault detection on line (m, n).

$$= \left(W_{(m,n)}[k] + \log \frac{f_{(m,n)}(\Delta I[k+1])}{f_0(\Delta I[k+1])}\right)^+$$
(32)

where $W_{(m,n)}[0] = 0$ and $(\cdot)^+ \triangleq \max\{0, \cdot\}$. Lastly, a fault/change point can be detected whenever

$$\max_{(m,n)\in\mathcal{E}} W_{(m,n)}[k] \ge A_{\mathsf{td}} \tag{33}$$

where A_{td} is a threshold, which can be approximated by

$$A_{\rm td} = \log\left(|\mathcal{E}|\beta\right) \tag{34}$$

to meet the false alarm constraint [38]. Therefore, if a large mean time to false alarm value β is chosen (i.e., low probability of false alarms) then the threshold should be set higher at the expense of longer detection delay $(\tau - \gamma)$ and vice-versa.

The line statistic $W_{(m,n)}[k]$ that crosses the threshold is declared to be the one at fault. A flowchart depicting the implementation of the CUSUM algorithm for series are fault detection is presented in Fig. 3, where $W_{(m,n)}[k+1]$ is calculated in an iterative manner.

The calculation of each test statistic $W_{(m,n)}$ can be simplified further by expanding (32), using the normal (11) and postfault (26) density functions, as follows:

$$W_{(m,n)}[k+1] = \left(W_{(m,n)}[k] + \underbrace{\log\sqrt{\frac{\det(\Sigma_0)}{\det(\Sigma_{(m,n)})}}}_{\text{slower rate}}\right)$$

$$-\frac{1}{2}(\Delta I[k+1])^{T}\left(\underbrace{\Sigma_{(m,n)}^{-1} - \Sigma_{0}^{-1}}_{\text{slower rate}}\right)(\Delta I[k+1])\right)^{+}.$$
(35)

The computationally demanding terms in (35) can be precomputed offline or at a slower rate, separate from the main algorithm loop, since multiple samples (P in Fig. 3) are required to estimate the covariance matrix of the node voltages, $\Upsilon \triangleq E[\Delta V[k]\Delta V[k]^T]$, needed for Σ_0 in (8) and $\Sigma_{(m,n)}$ in (23). Therefore, the computation of each $W_{(m,n)}$ consists mainly of multiplications and additions, which can be efficiently computed even for larger networks.

The overall series arc fault detection, identification, and clearing time is mainly decided by the threshold selection, where a lower threshold implies faster detection at the expense of possible false alarms and vice-versa. According to the UL1699B standard on photovoltaic series arc fault detection [64], the fault should be detected and cleared within 2.5 s or based on the following equation for high power systems:

$$T_{\text{det}} \le \min\left\{2.5, \frac{750}{I_{\text{arc}}V_{\text{arc}}}\right\} \tag{36}$$

where 750 J is the highest energy level at which a single arc fault exhibits low risk of fire [64], [65], $I_{\rm arc}$ is the arc current, and $V_{\rm arc}$ is the voltage across the arc fault. Using this equation, the detection/clearing time for high power systems (kW-MW) is around 1 s. The proposed detection and identification of series arc fault can be implemented much faster (\ll 100 ms) than the required UL1699B detection time, as shown in Section V.

B. Reduced Availability of Current Sensors

The algorithm in previous section requires the full set of nodal current measurements. However, we provide an approach to detect and identify a series arc fault at any line for the case when the number of sensors in a network are reduced. We can then relate the available measurements to the current vector by

$$\tilde{I} = CI \tag{37}$$

where $\tilde{I} \in \mathbb{R}^p, I \in \mathbb{R}^N$, and p < N. Therefore, it can be seen that

$$\Delta \tilde{I}[k] = CY\Delta V[k] = \tilde{Y}\Delta V[k] \tag{38}$$

where $\tilde{Y} \triangleq CY \in \mathbb{R}^{p \times N}.$ The prefault random variable can then be computed as

$$\Delta \tilde{I}[k] \sim \mathcal{N}\left(0_N, \ \tilde{\Sigma}_0\right)$$
 (39)

where the covariance $\tilde{\Sigma}_0 \in \mathbb{R}^{p \times p}$ is defined as $\tilde{\Sigma}_0 = \tilde{Y} \Upsilon \tilde{Y}^T$. The postfault random variable $\Delta \tilde{I}[k] \in \mathbb{R}^p$ is given by

$$\Delta \tilde{I}[k] \sim \mathcal{N}\left(0_N, \ \tilde{\Sigma}_{(m,n)}\right)$$
 (40)

where
$$\tilde{\Sigma}_{(m,n)} = \tilde{Y}_{(m,n)} \Upsilon \tilde{Y}_{(m,n)}^T + \psi \tilde{B}_{(m,n)} \tilde{B}_{(m,n)}^T \in \mathbb{R}^{p \times p},$$
 $\tilde{Y}_{(m,n)} = CY_{(m,n)} \in \mathbb{R}^{p \times N},$ and $\tilde{B}_{(m,n)} = CB_{(m,n)} \in \mathbb{R}^{p}.$

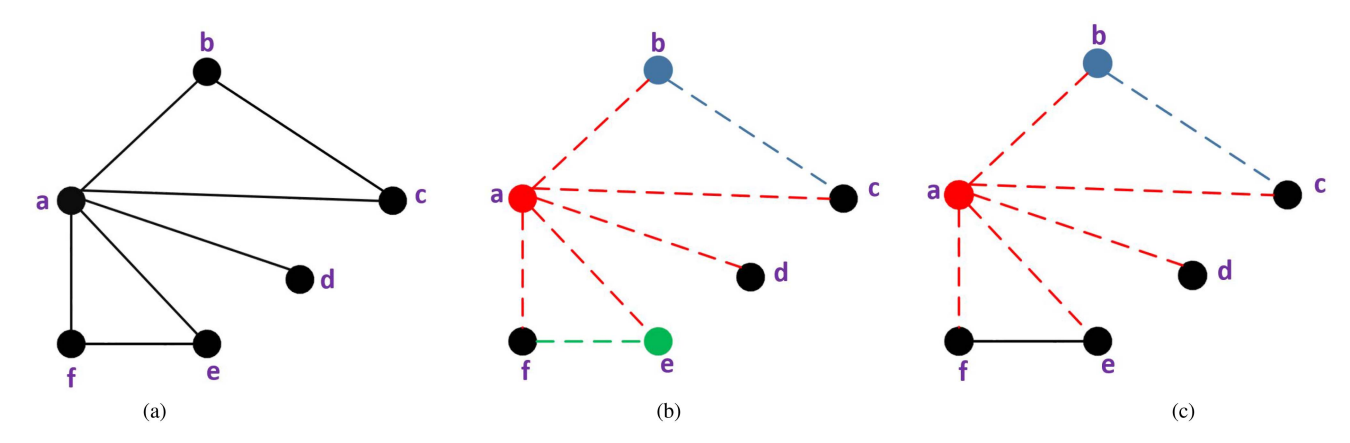


Fig. 4. Vertex cover example. Placing sensors at nodes {a, b, e} achieves observability of all of the lines. (a) Reference graph. (b) Edges incident to nodes $\{a, b, e\}$ (vertex cover). (c) Edges incident to nodes $\{a, b\}$. Edge (f, e) is not observable.

However, for any topology G, the sensor placement decided by the matrix $C \in \mathbb{R}^{p \times N}$ needs to be defined such that all line conductances $y_{(m,n)}$ are present in matrix \tilde{Y} . If a line conductance $y_{(m,n)}$ is eliminated from \tilde{Y} , it would cause the pre and postfault pdf for that particular edge/line to remain equal, since $\tilde{Y} = \tilde{Y}_{(m,n)}$. Therefore, for this case, it is not possible to identify a series arc fault at line (m, n).

The problem of deciding whether a fixed number of sensors can observe all of the lines in a network, i.e., all of the line conductances will be included in \hat{Y} , can be formulated as a vertex cover problem. A set $\mathcal{S} \subseteq \mathcal{V}$ is defined as a vertex cover if all of the lines in $\mathcal E$ are incident to at least one of the nodes in \mathcal{S} [66]. Moreover, every line/conductance value will be present in Y when the sensors are placed in S.

Fig. 4 shows an example of vertex cover on the graph presented in Fig. 4(a). When the sensors are placed at nodes $\{a, b, e\}$, all the lines in the network are observable, as shown in Fig. 4(b). However, when the sensors are placed only at nodes $\{a,b\}$, line (e,f) is not observable [see Fig. 4(c)]. We can now state the following proposition.

Proposition 1: Let $S \subseteq V$, $\Delta I[k]$ be the current injection measurements at the nodes in S, and $\Delta I[k] = Y\Delta V$. If S is a vertex cover set, then $\tilde{Y} = CY$ contains information on the conductance of all of the lines.

Proof: From the nodal equation (2), the matrix Y is a weighted Laplacian matrix, where the ith row contains the line conductances of all edges incident to node i. Given $\tilde{Y} = CY$, where the matrix C selects only the rows of the nodes in S, we can conclude that rows of \tilde{Y} also consists of line conductances of all edges incident to each node in S. Lastly, since S is assumed to be a vertex cover set, \tilde{Y} contains information on the conductances of all the lines.

Finding the minimum vertex cover set is useful for deciding the minimum number and location of sensors required to detect and identify a series arc fault at any line. For this purpose, a greedy algorithm is presented to find the minimum set of sensors required or minimum vertex cover for a given dc network. At the first iteration, the set of nodes of the original graph/network, $\mathcal{G}^1 = (\mathcal{V}^1, \mathcal{E}^1)$, is arranged in terms of decreasing degree, i.e., the number of edges incident to each node. For example, in the

Algorithm 1: Greedy Algorithm for Finding Minimum Vertex Cover Set.

- Define $\mathcal{G}_1 = \{\mathcal{V}^1, \mathcal{E}^1\}$
- Re-arrange the nodes in \mathcal{V}^1 in terms of decreasing the
- Define vector $S = \{\}$ to store optimal nodes 3:
- 4: Set j = 1
- while $\delta[\mathcal{V}_1^j] \neq 0$ do 5:
- Store V_1^j in S
- 7:
- Define $\mathcal{G}_{j+1} = \mathcal{G}_j \mathcal{V}_1^j = \{\mathcal{V}^{j+1}, \ \mathcal{E}^{j+1}\}$ Arrange the nodes in \mathcal{V}^{j+1} in terms of decreasing 8:
- 9: Set j = j + 1
- 10: end while
- S is a vertex cover set

first iteration $\mathcal{V}^1 = \{\mathcal{V}^1_1, \, \mathcal{V}^1_2, \, \cdots, \, \mathcal{V}^1_N\}$, where the degree of each node satisfy

$$\delta[\mathcal{V}_1^1] \ge \delta[\mathcal{V}_2^1] \ge \dots \ge \delta[\mathcal{V}_N^1] \tag{41}$$

where $\delta[\mathcal{V}_i^j]$ represents the degree of node \mathcal{V}_i^j and j is the iteration step. The node with highest degree, V_1^1 , is then stored in the optimal sensor placement set, S.

In the next iteration, define the graph $\mathcal{G}_2 \triangleq (\mathcal{V}^2, \mathcal{E}^2)$ as $\mathcal{G}_2 \triangleq$ $\mathcal{G}_1 - \mathcal{V}_1^1$. This leads to a reduction of degree by one for the set of nodes adjacent to \mathcal{V}_1^1 . The set of nodes \mathcal{V}^2 is then rearranged in terms of decreasing degree, similar to (41), and \mathcal{V}_1^2 is stored in S. We proceed in this manner until $\delta[\mathcal{V}_1^k] = 0$ for some step k. The set of nodes stored in S forms a minimum vertex cover set. This algorithm is summarized in Algorithm 1.

At certain iterations, it is possible to obtain multiple nodes with maximum degree, i.e., the first inequalities are binding in (41). In this case, multiple minimum vertex cover sets can be obtained by choosing one node over the other. If several solutions to the minimum vertex cover set are obtained using the greedy algorithm multiple times, the KL divergence, i.e., the relative entropy of two distributions, can be used to find an optimal set of sensors. For the CUSUM algorithm, the worst-case average detection delay (WADD) for testing a change from f_0 (normal) to $f_{(m,n)}$ [fault at line (m,n)] is given by [67]

WADD
$$\sim \frac{\log \beta}{D(f_{(m,n)}||f_0)}$$
. (42)

Therefore, it can be seen that for a fixed β , a larger KL divergence $D(f_{(m,n)}||f_0)$ implies a smaller detection delay. Consider the prefault distribution, $f_0(x) \sim \mathcal{N}(0, \Sigma_0)$, and the distribution with a fault at line (m, n), $f_{(m,n)}(x) \sim \mathcal{N}(0, \Sigma_{(m,n)})$, the KL divergence between these two distributions can be obtained as

$$D(f_{(m,n)}||f_0)$$

$$= \frac{1}{2} \left[\operatorname{tr} \left(\Sigma_0^{-1} \Sigma_{(m,n)} \right) - p + \log \left(\det \left(\Sigma_0 \Sigma_{(m,n)}^{-1} \right) \right) \right] \tag{43}$$

where p is the number of sensors being used. Therefore, assuming that there are K minimum vertex cover sets, an optimal sensor placement can be chosen by a solution to the following problem:

$$\max_{1 \le k \le K} \left[\min_{(m,n) \in \mathcal{E}} \left(D(f_{(m,n)} || f_0) \right)_k \right] \tag{44}$$

where the superscript k denotes the index of a specific minimum vertex cover set. In this problem, the set of sensors that maximizes the smallest KL divergence of a certain line is chosen, improving the detection time for the worst-case scenario.

C. Internal Node Elimination

In this section, the QCD algorithm is formulated for the case when the microgrid has internal nodes, i.e., buses without loads, sources, or capacitors. Kron reduction is used to further simplify the nodal equations by eliminating the internal nodes [68]. The prefault nodal equation for this case can be written as

$$\begin{pmatrix} \Delta I_{\alpha} \\ 0_{|\beta|} \end{pmatrix} = \begin{pmatrix} Y_{\alpha,\alpha} & Y_{\alpha,\beta} \\ Y_{\beta,\alpha} & Y_{\beta,\beta} \end{pmatrix} \begin{pmatrix} \Delta V_{\alpha} \\ \Delta V_{\beta} \end{pmatrix} \tag{45}$$

where $\alpha \subseteq \mathcal{V}$ is the set of nodes that have at least one source or load connection to each bus, while $\beta \subset \mathcal{V}$ defines the set of internal nodes, i.e., without sources, loads, or capacitors. Therefore, it can be seen that $\alpha \cup \beta = \mathcal{V}$. The vector ΔI_{α} are the injection currents at the set of nodes defined by α , and $0_{|\beta|}$ is a column vector of zeros with dimension $|\beta|$ defining the zero current injection at the set of nodes in β (internal nodes). In order to eliminate the nodes in β , we can use the second row in (45)

$$0_{|\beta|} = Y_{\beta,\alpha} \Delta V_{\alpha} + Y_{\beta,\beta} \Delta V_{\beta} \tag{46}$$

where we can solve for ΔV_{β} as

$$\Delta V_{\beta} = -\left[Y_{\beta,\beta}\right]^{-1} Y_{\beta,\alpha} \Delta V_{\alpha} \tag{47}$$

and substitute in (45)

$$\Delta I_{\alpha} = Y_{\alpha,\alpha} \Delta V_{\alpha} - Y_{\alpha,\beta} \left([Y_{\beta,\beta}]^{-1} Y_{\beta,\alpha} \Delta V_{\alpha} \right)$$

$$\Rightarrow \Delta I_{\alpha} = \left(Y_{\alpha,\alpha} - Y_{\alpha,\beta} \left[Y_{\beta,\beta} \right]^{-1} Y_{\beta,\alpha} \right) \Delta V_{\alpha}. \tag{48}$$

TABLE I DC MICROGRID LINE PARAMETERS

Line	(1,2)	(2,4)	(2,5)	(2,6)	(3,4)	(4,7)	(4,8)
$r_{(i,j)} (\mathrm{m}\Omega)$	3.2	0.8	3.2	3.2	3.2	3.2	3.2
$L_{(i,j)}^{(i,j)}$ (μ H)	5.5	1.37	5.5	5.5	5.5	5.5	5.5

The random variable ΔI_{α} defined during prefault scenario is then given by

$$\Delta I_{\alpha} = \tilde{Y} \Delta V_{\alpha} \tag{49}$$

where $\tilde{Y}=Y_{\alpha,\alpha}-Y_{\alpha,\beta}[Y_{\beta,\beta}]^{-1}Y_{\beta,\alpha}$. The postfault nodal equation for a series arc fault at line $(m, n) \in \mathcal{E}$ is given by

$$\begin{pmatrix} \Delta I_{\alpha} \\ 0_{|\beta|} \end{pmatrix} = \begin{pmatrix} Y_{\alpha,\alpha(m,n)} & Y_{\alpha,\beta(m,n)} \\ Y_{\beta,\alpha(m,n)} & Y_{\beta,\beta(m,n)} \end{pmatrix} \begin{pmatrix} \Delta V_{\alpha} \\ \Delta V_{\beta} \end{pmatrix} + \begin{pmatrix} P_{\alpha} \\ P_{\beta} \end{pmatrix} \Delta V_{\text{arc}}.$$
(50)

The vectors P_{α} and P_{β} are column vectors of zeros with $-y_{(m,n)\gamma}$ and $y_{(m,n)\gamma}$ at mth and nth node's index, respectively. We can similarly solve for ΔV_{β} as

$$\Delta V_{\beta} = -Y_{\beta,\beta(m,n)}^{-1} \left[Y_{\beta,\alpha(m,n)} \Delta V_{\alpha} + P_{\beta} \Delta V_{\text{arc}} \right]$$
 (51)

and substitute in (50) to obtain

$$\Delta I_{\alpha} = \tilde{Y}_{(m,n)} \Delta V_{\alpha} + \tilde{P}_{(m,n)} \Delta V_{\text{arc}}$$
 (52)

$$\tilde{Y}_{(m,n)} = Y_{\alpha,\alpha(m,n)} - Y_{\alpha,\beta(m,n)} \left(\left[Y_{\beta,\beta(m,n)} \right]^{-1} Y_{\beta,\alpha(m,n)} \right)$$
(53)

and $\tilde{P}_{(m,n)}=-Y_{\alpha,\beta(m,n)}Y_{\beta,\beta(m,n)}^{-1}P_{\beta}+P_{\alpha}$. The pdf for both the pre and postfault ΔI_{α} can be obtained using (49) and (52).

The greedy algorithm and the internal node elimination presented in Section III-B and III-C, respectively are independent of each other. For example, if there are no internal nodes in the dc microgrid presented in Fig. 1 (i.e., load connections are provided at nodes 2 and 4), then by only applying the greedy algorithm to the microgrid with parameters given in Table I, we obtain nodes 2 and 4 to be the optimal positions to place the currents sensors, i.e., they form a minimum vertex cover. This case will be discussed in the next section.

IV. SIMULATION RESULTS

In this section, simulation results are presented for a typical more electric aircraft's dc microgrid [51], [53] using MATLAB Simulink with the SimPowerSystems toolbox. The microgrid is presented in Fig. 1 and can be modeled as a graph $\mathcal{G} = (\mathcal{V}, \mathcal{E})$, with $|\mathcal{V}| = 8$ (nodes) and $|\mathcal{E}| = 7$ (lines). The line resistances and inductances used in all cases are given in Table I. The sources and loads are modeled using buck converters using standard cascaded control (inner current and outer voltage loop) [69]. The switching frequency of all converters is set to $F_{\rm sw}=20~{\rm kHz}$. The nominal output voltage of the source converters is $V_{\rm dc} = 400 \text{ V}$. The simulation time step is set to $T_{\text{sim}} = 1 \ \mu\text{s}$. For all cases, the CUSUM algorithm's time step is set to $T_{\rm OCD}=1$ ms. This

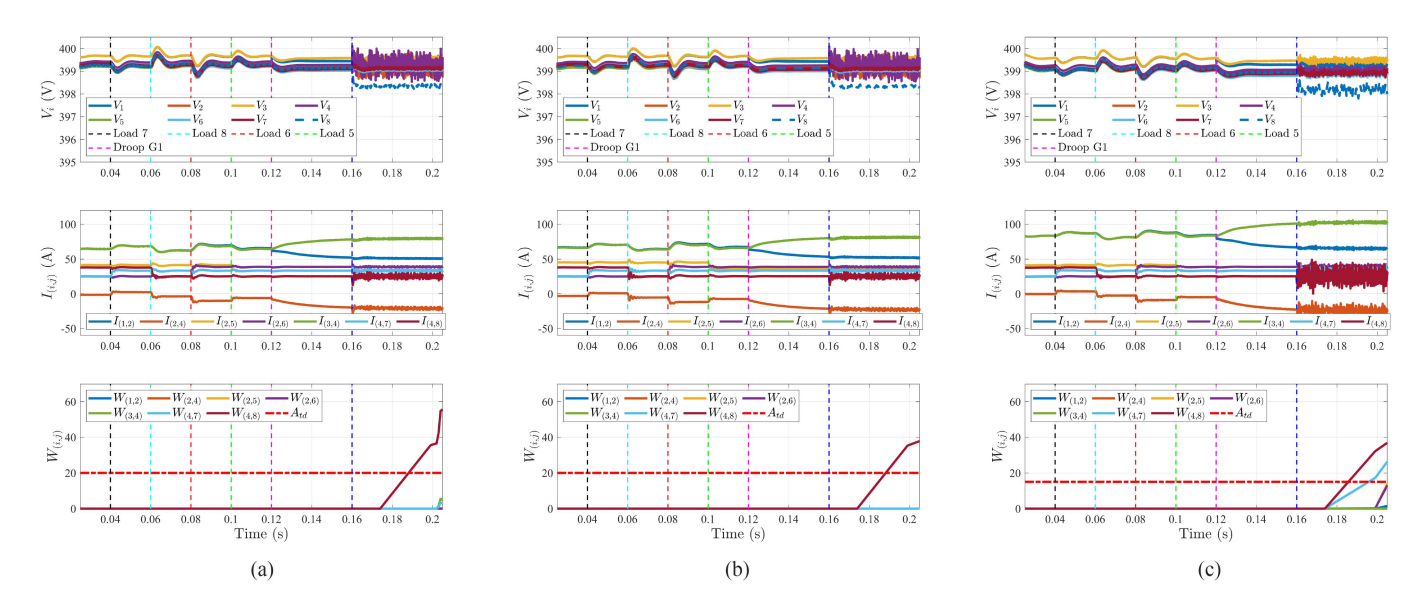


Fig. 5. Simulation results for all three cases. *Top:* node voltages, *middle:* line currents, *bottom:* CUSUM statistics. (a) Case 1: Series arc fault detection on line (4, 8). (b) Case 2: Series arc fault detection on line (4, 8).

time step is decided based the recommendation of being approximately equal to the largest line time constant (1.7 ms), without sacrificing a large increase in detection delay. The following three case studies are considered.

- 1) Case 1: Kron reduction is applied on the microgrid shown in Fig. 1 to eliminate the two internal nodes 2 and 4. The current sensors are then placed at all remaining nodes {1, 3, 5, 6, 7, 8}.
- 2) Case 2: In this case, Kron reduction is followed by the application of minimum vertex cover strategy on the microgrid presented in Fig. 1. In this case, sensors are placed only at nodes {3, 5, 6, 7, 8} (i.e., nodes 1, 2, and 4 are eliminated).
- 3) Case 3: In this case, nodes 2 and 4 in Fig. 1 are now connected to constant power loads (CPLs) such that no internal nodes are present. Using Algorithm 1, only current sensors at nodes 2 and 4 (minimum vertex cover) are used.

In cases 1 and 3, the loads connected to nodes 5–8 are of CPL, constant current load (CCL), CPL, and CPL-type, respectively. In case 2, the load at node 8 is substituted with a resistive load. Although the majority of loads in aircraft power systems are of the CPL type [70], [71], we consider a combination of all three load types to better represent more general systems [72]. In all cases, a series arc fault is triggered on line (4, 8) at time $\gamma = 0.16$ s, the case studies also include testing of the proposed CUSUM algorithm during nominal operating conditions. The following load changes were implemented on the dc microgrid.

- 1) Node 7: Change in load power from 10 to 13.2 kW at t = 0.04 s.
- 2) Node 8: Change in load power from 15 to 10 kW at t = 0.06 s.
- 3) Node 6: Change in load power from 9900 W to 15.4 kW at t = 0.08 s.
- 4) Node 5: Change in load power from 16.4 to 13.2 kW at $t=0.1~\mathrm{s}$.

5) Node 1: Change in generator output power from 27 to 23 kW at t = 0.12 s (by changing droop gain).

The nodal voltages and line currents for cases 1–3 are presented in Fig. 5(a)–(c) (top, middle, and bottom subfigures), respectively.

A. Case 1: System With CPL, CCL, and Internal Node Elimination

In this section, the dc microgrid presented in Fig. 1 is used with the internal nodes 2 and 4 eliminated using Kron reduction. Current sensors are then placed at nodes 1, 3, and 5–8. The loads at nodes 5–8 are of CPL, CCL, CPL, and CPL-type, respectively. The series arc fault detection on line (4, 8) is presented in Fig. 5(a), where the threshold $A_{\rm td}$ is set to 20, and the series arc fault is triggered at time $\gamma=0.16$ s on line (4, 8). Finally, the series arc fault is said to be detected at a certain time τ , when the value of $W_{(4,8)}$ crosses the threshold $A_{\rm td}$, as shown in Fig. 5(a) (bottom subfigure). Furthermore, Fig. 5(a) shows that the CUSUM statistics remains unaffected by load changes.

B. Case 2: System With CPLs, CCL, and Resistive Load With Internal Node Elimination and Optimal Sensor Placement

In this case, Kron reduction is followed by the application of vertex cover strategy (see Algorithm 1) on the microgrid presented in Fig. 1. The current sensor placement after applying the two strategies are 3, 5, 6, 7, and 8 (nodes 1, 2, and 4 are now excluded) and is obtained from the KL divergence analysis discussed in Section III-B. The series are fault detection on line (4, 8) is presented in Fig. 5(b) where $A_{\rm td}=20$ and $\gamma=0.16$ s. It can also be seen that the CUSUM statistics, $W_{m,n}[k] \ \forall (m,n) \in \mathcal{E}$, are not affected by the load changes. The series are fault is said to be detected when $W_{(4,8)}[k] \geq A_{td}$. It can be seen that the detection delay is approximately equal to case 1, even with one sensor removed.

TABLE II $\label{eq:table_eq} \text{Detection Delay for Each Line With Threshold } A_{\text{TD}} = 20$

Case 1	Case 2	Case 3	
τ_d (ms)	τ_d (ms)	τ_d (ms)	
27	27	17	
109	105	110	
27	27	23	
26	26	23	
25	26	16	
27	27	25	
29	29	26	
	$ au_d ext{ (ms)}$ 27 109 27 26 25 27	$ \begin{array}{c cccc} \tau_d \ (\text{ms}) & \tau_d \ (\text{ms}) \\ \hline 27 & 27 \\ \hline 109 & 105 \\ \hline 27 & 27 \\ \hline 26 & 26 \\ \hline 25 & 26 \\ \hline 27 & 27 \\ \hline \end{array} $	

C. Case 3: System With CPLs, CCL, and Optimal Sensor Placement

In this case, the nodes 2 and 4 in Fig. 1 are connected to CPLs with a base power of 7 and 8 kW respectively, such that no internal nodes are present in this network. The vertex cover strategy using the greedy algorithm discussed in Section III-B is applied and the minimum vertex cover set is given by the set $\mathcal{S} = \{2, 4\}$. Therefore, only current sensors at these nodes are used. The series arc fault was set to trigger at time $\gamma = 0.16$ s on line (4, 8) and the fault is detected when $W_{4,8} \geq A_{\rm td} = 20$, as seen in Fig. 5(c). It is also to be noted that the load changes/nominal dc microgrid operations do not affect the CUSUM algorithm-based series arc fault detection. In addition, while other statistics also increased, the fault is detected and decided to be at the one which first crosses the threshold.

D. Detection Delay

The detection delay is defined as the amount of time it takes for the statistic $W_{(i,j)}$ to cross over a predefined threshold $(A_{\rm td})$ after the fault has started, as shown in (33). To compare the detection delay between all three cases, a fixed series arc variance and threshold is set for all lines. The load power varies as specified in the previous cases. Simulations are then conducted for a fault at each line and the detection delay is obtained for each line, as given in Table II.

We can directly compare cases 1 and 2 since they have the same number and type of sources and loads. While both have a similar detection delay, case 1 is slightly faster for line (3,4) and slower for line (2,4). In case 3, two loads were added to nodes 2 and 4. It can be seen that this case also has a comparable detection delay while using less number of sensors. Lastly, line (2,4) has the highest detection delay for all the cases. The detection delays were obtained by setting a threshold value of $A_{\rm td}=20$. A smaller threshold can reduce the detection delay at the expense of possible false alarms.

V. EXPERIMENTAL RESULTS

A four node dc microgrid testbed was built for experimental verification of the proposed QCD-based algorithm. A schematic representation of the testbed is presented in Fig. 6, and the

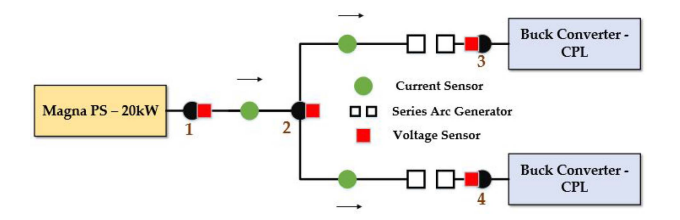


Fig. 6. Four node microgrid used in experimental results.

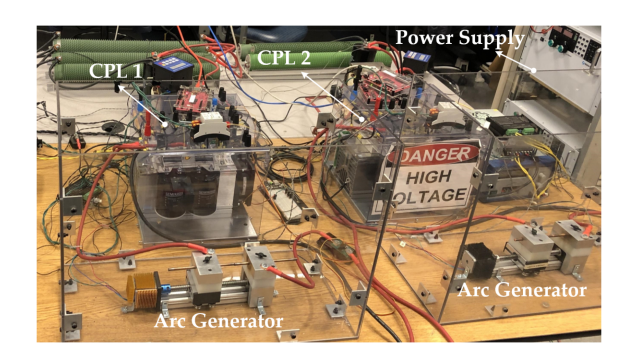


Fig. 7. Hardware setup for experimental results.

TABLE III TESTBED LINE PARAMETERS

Line	(1,2)	(2,3)	(2,4)	
$r_{(i,j)} (\mathrm{m}\Omega)$	8.7	4.2	2.4	
$L_{(i,j)}$ (μ H)	7.5	3.6	2.1	

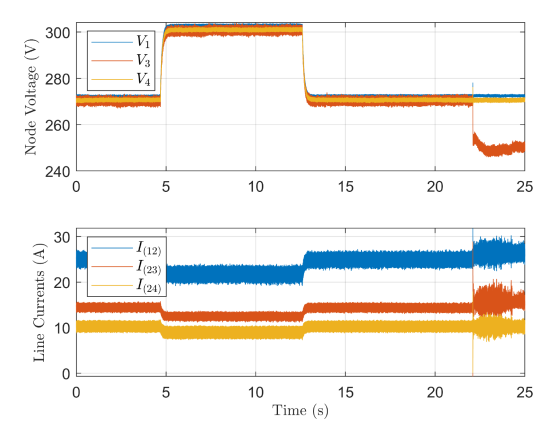


Fig. 8. Experimental results—voltage and injection current measurements during a fault in line (2,3) at $t=0.267~\rm s.$

hardware setup is shown in Fig. 7. The input voltage to the network uses a 20-kW Magna dc power supply [73]. The nominal bus voltage output is 270 V. The loads connected to nodes 3 and 4 are designed using closed loop controlled buck converters (cascaded proportional integral (PI) control) to represent CPLs using a Semikron silicon-based insulated gate bipolar transistors (IGBTs) [74]. The switching frequency of the converters is set to 10 kHz. The line parameters are given in Table III.

The voltage and current measurements were sampled at a time step of 8 μ s while the CUSUM algorithm is operated at a time step of 160 μ s. The node voltages and the line currents are shown in Fig. 8 and the experimental results are shown in Fig. 9. A

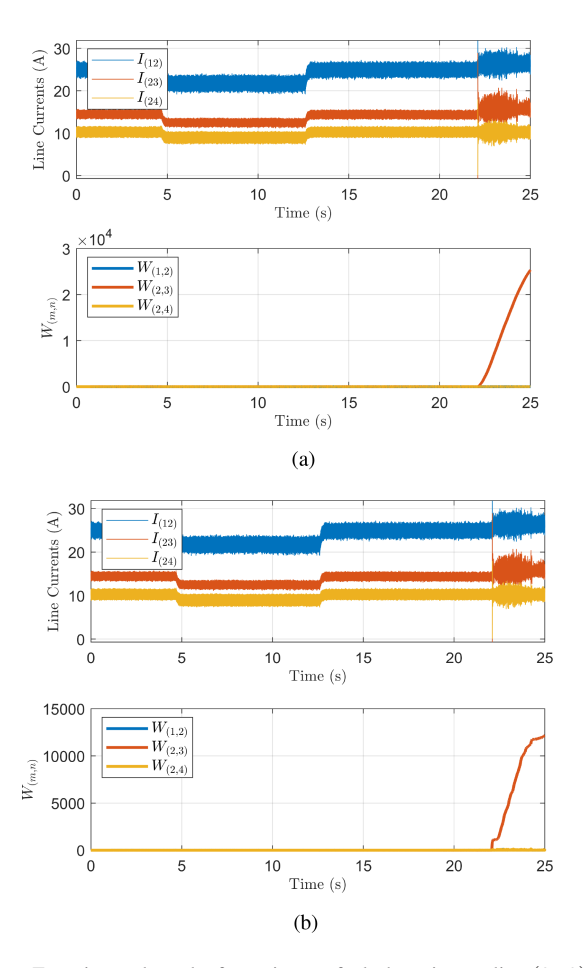


Fig. 9. Experimental results for series arc fault detection on line (2, 3). (a) Case 1: Elimination of current sensor at node 2. (b) Case 2: Fault detection with sensors only at nodes 3 and 4 (optimal sensor placement).

current change is initiated at nodes 3 and 4, where the current is dropped to 12.5 and 9 A from 15 and 10 A, respectively, at $t=4.69~\rm s$, by changing the input voltage reference from 270 to 300 V, respectively. Next, at $t=12.6~\rm s$ the load currents at nodes 3 and 4 are brought back to 15 and 10 A, respectively, by setting the input voltage to the original value of 270 V. Finally, at $t=22.103~\rm s$, the series are fault was triggered on line (2,3), which can be seen in Fig. 8, where the arc noise affects all of the line currents.

A. Case 1: Internal Node Elimination

In this case, fault detection is achieved by performing internal node elimination by Kron reduction. Since a load or generator is absent at node 2, the following sets are defined:

$$\alpha = \{1, 3, 4\} \quad \beta = \{2\} \tag{54}$$

where β contains the internal node. By formulating (49) and (52) for the CUSUM algorithm, the series arc fault detection on line (2, 3) can be successfully achieved, as shown in Fig. 9(a), where once the fault is triggered at t=22.103 s, the CUSUM metric $W_{(2,3)}$ increases rapidly. Furthermore, it is also shown that the load current changes at nodes 3 and 4 (t=4.69 s and t=12.6 s), by varying the input voltage, do not affect the CUSUM's detection statistic $W_{(m,n)}[k]$.

B. Case 2: Reduced Information

In addition to the Kron reduction for internal node elimination, as shown in Section V-A, the vertex cover algorithm can be applied to minimize the number of current sensors deployed over the testbed while also maintaining complete observability of all the lines. Furthermore, the KL divergence criterion in (44) is also used for the best possible series arc fault detection. Therefore, applying the vertex cover method to the Kron reduced model obtained from Section V-A, the CUSUM algorithm is operated by only using two current sensors at nodes 3 and 4 [solutions to the KL divergence criterion in (44)]. The series arc fault triggered on line (2, 3) at t = 22.103 s is successfully detected even after reducing the number of sensors, as seen in Fig. 9(b). However, it can be seen that the fault detection delay is longer in Fig. 9(b) compared with Fig. 9(a), which can be verified by the magnitude of $W_{(2,3)}$ at t=25 s. In Fig. 9(a), the magnitude of $W_{(2,3)}$ is 25 000 and in Fig. 9(b) is 12 000. Hence, a larger number of sensors improves the detection delay in this case.

VI. CONCLUSION

This article addresses the problem of detecting and identifying series arc faults in dc microgrids used in the more electric aircraft, using QCD and the CUSUM algorithm. The dc microgrid's nodal equation and the noise induced by the series arc fault are used to determine the pre and postfault data generating distributions. In addition, an algorithm is presented to determine the minimum number of sensors needed to detect and identify faults at any line using the minimum vertex cover problem, and a Kron reduction method is shown to eliminate internal nodes and further reduce the sensors in a network. Simulation and experimental results are shown, where the Kron reduction approach is applied to eliminate the internal nodes and a case study with reduced current sensor availability is explored to validate the CUSUM algorithm's ability to detect a series arc fault on a dc microgrid.

For future work, dynamic faults comprising multiple stages, such as arc initiation, intermittent, steady state, isolation, and reconfiguration will be considered. In addition, analysis of robustness of the algorithm to parameter variations will be conducted using robust QCD methods. Moreover, distributed and/or decentralized QCD-based techniques will also be explored to reduce the number of computations for larger networks. Lastly, the proposed methods will be extended to other applications, such as utility scale dc networks.

REFERENCES

- K. M. Armijo, J. Johnson, M. Hibbs, and A. Fresquez, "Characterizing fire danger from low-power photovoltaic arc-faults," in *Proc. IEEE 40th Photovolt. Specialist Conf.*, 2014, pp. 3384–3390.
- [2] M. Naidu, T. J. Schoepf, and S. Gopalakrishnan, "Arc fault detection scheme for 42-V automotive DC networks using current shunt," *IEEE Trans. Power Electron.*, vol. 21, no. 3, pp. 633–639, May 2006.
- [3] J. Johnson et al., "Photovoltaic DC arc fault detector testing at Sandia National Laboratories," in *Proc. 37th IEEE Photovolt. Specialists Conf.*, 2011, pp. 003614–003619.
- [4] X. Yao, L. Herrera, S. Ji, K. Zou, and J. Wang, "Characteristic study and time-domain discrete- wavelet-transform based hybrid detection of series DC arc faults," *IEEE Trans. Power Electron.*, vol. 29, no. 6, pp. 3103–3115, Jun. 2014.

- [5] X. Yao, "Study on DC arc faults in ring-bus DC microgrids with constant power loads," in Proc. IEEE Energy Convers. Congr. Expo., 2016, pp. 1–5.
- [6] Y. Abdullah et al., "Hurst-exponent-based detection of high-impedance DC are events for 48-V systems in vehicles," *IEEE Trans. Power Electron.*, vol. 36, no. 4, pp. 3803–3813, Apr. 2021.
- [7] J. C. Kim, B. Lehman, and R. Ball, "A series DC arc fault detection algorithm based on PV operating characteristics and detailed extraction of pink noise behavior," in *Proc. IEEE Appl. Power Electron. Conf. Expo.*, 2021, pp. 989–994.
- [8] J.-B. Ahn, H.-B. Jo, and H.-J. Ryoo, "Real-time DC series arc fault detection based on noise pattern analysis in photovoltaic system," *IEEE Trans. Ind. Electron.*, vol. 70, no. 10, pp. 10680–10689, Oct. 2023.
- [9] W. Miao, X. Liu, K. H. Lam, and P. W. T. Pong, "Arc-faults detection in PV systems by measuring pink noise with magnetic sensors," *IEEE Trans. Magn.*, vol. 55, no. 7, Jul. 2019, Art. no. 4002506.
- [10] S. Chen, H. Wu, Y. Meng, Y. Wang, X. Li, and C. Zhang, "Reliable detection method of variable series arc fault in building integrated photovoltaic systems based on nonstationary time series analysis," *IEEE Sensors J.*, vol. 23, no. 8, pp. 8654–8664, Apr. 2023.
- [11] A. Amiri, H. Samet, and T. Ghanbari, "Recurrence plots based method for detecting series are faults in photovoltaic systems," *IEEE Trans. Ind. Electron.*, vol. 69, no. 6, pp. 6308–6315, Jun. 2022.
- [12] M. Jalil, H. Samet, and T. Ghanbari, "Dynamic polynomial models with ARMA coefficients used for modeling the DC series are fault in photovoltaic systems," *IEEE Trans. Ind. Informat.*, vol. 19, no. 5, pp. 6364–6375, May 2023.
- [13] Z. Wang and R. S. Balog, "Arc fault and flash signal analysis in DC distribution systems using wavelet transformation," *IEEE Trans. Smart Grid*, vol. 6, no. 4, pp. 1955–1963, Jul. 2015.
- [14] Y.-L. Shen and R.-J. Wai, "Wavelet-analysis-based singular-value-decomposition algorithm for weak arc fault detection via current amplitude normalization," *IEEE Access*, vol. 9, pp. 71535–71552, 2021.
- [15] Q. Xiong et al., "Series are fault detection and localization in DC distribution system," *IEEE Trans. Instrum. Meas.*, vol. 69, no. 1, pp. 122–134, Jan. 2020.
- [16] J. Gu, D. Lai, J. Wang, J. Huang, and M. Yang, "Design of a DC series are fault detector for photovoltaic system protection," *IEEE Trans. Ind. Appl.*, vol. 55, no. 3, pp. 2464–2471, May/Jun. 2019.
- [17] R. D. Telford, S. Galloway, B. Stephen, and I. Elders, "Diagnosis of series DC are faults-A machine learning approach," *IEEE Trans. Ind. Informat.*, vol. 13, no. 4, pp. 1598–1609, Aug. 2017.
- [18] V. Le, X. Yao, C. Miller, and B.-H. Tsao, "Series DC arc fault detection based on ensemble machine learning," *IEEE Trans. Power Electron.*, vol. 35, no. 8, pp. 7826–7839, Aug. 2020.
- [19] V. Le and X. Yao, "Ensemble machine learning based adaptive arc fault detection for DC distribution systems," in *Proc. IEEE Appl. Power Electron. Conf. Expo.*, 2019, pp. 1984–1989.
- [20] S. Lu, T. Sirojan, B. Phung, D. Zhang, and E. Ambikairajah, "DA-DCGAN: An effective methodology for DC series arc fault diagnosis in photovoltaic systems," *IEEE Access*, vol. 7, pp. 45831–45840, 2019.
- [21] Y. Wang, L. Hou, K. C. Paul, Y. Ban, C. Chen, and T. Zhao, "ArcNet: Series AC arc fault detection based on raw current and convolutional neural network," *IEEE Trans. Ind. Informat.*, vol. 18, no. 1, pp. 77–86, Jan. 2022.
- [22] Y. Sung, G. Yoon, J.-H. Bae, and S. Chae, "TL-LEDarcNet: Transfer learning method for low-energy series DC arc-fault detection in photovoltaic systems," *IEEE Access*, vol. 10, pp. 100725–100735, 2022.
- [23] J. Yan, Q. Li, and S. Duan, "A simplified current feature extraction and deployment method for DC series are fault detection," *IEEE Trans. Ind. Electron.*, vol. 71, no. 1, pp. 625–634, Jan. 2024.
- [24] H.-L. Dang, J. Kim, S. Kwak, and S. Choi, "Series DC arc fault detection using machine learning algorithms," *IEEE Access*, vol. 9, pp. 133346–133364, 2021.
- [25] H.-L. Dang, S. Kwak, and S. Choi, "Identifying DC series and parallel arcs based on deep learning algorithms," *IEEE Access*, vol. 10, pp. 76386–76400, 2022.
- [26] L. Xing, Y. Wen, S. Xiao, D. Zhang, and J. Zhang, "A deep learning approach for series DC arc fault diagnosing and real-time circuit behavior predicting," *IEEE Trans. Electromagn. Compat.*, vol. 64, no. 2, pp. 569–579, Apr. 2022.
- [27] Z. Yin, L. Wang, S. Yang, and Y. Gao, "A series are fault diagnosis method in DC distribution systems based on multiscale features and random forests," *IEEE Sensors J.*, vol. 23, no. 3, pp. 2605–2617, Feb. 2023.
- [28] V. Le, C. Miller, B.-H. Tsao, and X. Yao, "Series are fault identification in DC distribution based on random forest predicted probability," *IEEE Trans. Emerg. Sel. Topics Power Electron.*, early access, Dec. 12, 2022, doi: 10.1109/JESTPE.2022.3228421.

- [29] S. Dhar, R. K. Patnaik, and P. K. Dash, "Fault detection and location of photovoltaic based DC microgrid using differential protection strategy," *IEEE Trans. Smart Grid*, vol. 9, no. 5, pp. 4303–4312, Sep. 2018.
- [30] A. Shekhar, L. Ramírez-Elizondo, S. Bandyopadhyay, L. Mackay, and P. Bauera, "Detection of series arcs using load side voltage drop for protection of low voltage DC systems," *IEEE Trans. Smart Grid*, vol. 9, no. 6, pp. 6288–6297, Nov. 2018.
- [31] X. Yao, V. Le, and I. Lee, "Unknown input observer-based series DC are fault detection in DC microgrids," *IEEE Trans. Power Electron.*, vol. 37, no. 4, pp. 4708–4718, Apr. 2022.
- [32] K. Gajula and L. Herrera, "Detection and localization of series are faults in DC microgrids using Kalman filter," *IEEE Trans. Emerg. Sel. Topics Power Electron.*, vol. 9, no. 3, pp. 2589–2596, Jun. 2021.
- [33] K. Gajula, X. Yao, and L. Herrera, "Dual state-parameter estimation for series arc fault detection on a DC microgrid," in *Proc. IEEE Energy Convers. Congr. Expo.*, 2020, pp. 4649–4655.
- [34] V. V. Veeravalli and T. Banerjee, "Quickest change detection," in *Academic Press Library in Signal Processing*, vol. 3. Amsterdam, The Netherlands: Elsevier, 2014, pp. 209–255.
- [35] A. Tartakovsky, I. Nikiforov, and M. Basseville, Sequential Analysis: Hypothesis Testing and Changepoint Detection. (Series Monographs on Statistics and Applied Probability 136). London, U.K.: Chapman & Hall, 2015.
- [36] H. V. Poor and O. Hadjiliadis, *Quickest Detection*. New York, NY, USA: Cambridge Univ. Press, 2008.
- [37] L. Xie, S. Zou, Y. Xie, and V. V. Veeravalli, "Sequential (quickest) change detection: Classical results and new directions," *IEEE J. Sel. Areas Inf. Theory*, vol. 2, no. 2, pp. 494–514, Jun. 2021.
- [38] Y. C. Chen, T. Banerjee, A. D. Dominguez-Garcia, and V. V. Veeravalli, "Quickest line outage detection and identification," *IEEE Trans. Power Syst.*, vol. 31, no. 1, pp. 749–758, Jan. 2015.
- [39] G. Rovatsos, X. Jiang, A. D. Domínguez-García, and V. V. Veeravalli, "Comparison of statistical algorithms for power system line outage detection," in *Proc. IEEE Int. Conf. Acoust. Speech Signal Process.*, 2016, pp. 2946–2950.
- [40] G. Rovatsos, X. Jiang, A. D. Domínguez-García, and V. V. Veeravalli, "Statistical power system line outage detection under transient dynamics," *IEEE Trans. Signal Process.*, vol. 65, no. 11, pp. 2787–2797, Jun. 2017.
- [41] J. Heydari and A. Tajer, "Quickest localization of anomalies in power grids: A stochastic graphical approach," *IEEE Trans. Smart Grid*, vol. 9, no. 5, pp. 4679–4688, Sep. 2018.
- [42] T. Christman, N. Uhrich, P. Swisher, and X. Jiang, "A statistical approach for line outage detection in power systems with transient dynamics," in *Proc. IEEE Int. Conf. Probabilistic Methods Appl. Power Syst.*, 2018, pp. 1–5.
- [43] X. Jiang, Y. C. Chen, V. V. Veeravalli, and A. D. Domínguez-García, "Quickest line outage detection and identification: Measurement placement and system partitioning," in *Proc. North Amer. Power Symp.*, 2017, pp. 1–6.
- [44] L. Chen, S. Li, and X. Wang, "Quickest fault detection in photovoltaic systems," *IEEE Trans. Smart Grid*, vol. 9, no. 3, pp. 1835–1847, May 2018.
- [45] S. Li and X. Wang, "Cooperative change detection for voltage quality monitoring in smart grids," *IEEE Trans. Inf. Forensics Secur.*, vol. 11, no. 1, pp. 86–99, Jan. 2016.
- [46] M. N. Kurt, Y. Yilmaz, and X. Wang, "Distributed quickest detection of cyber-attacks in smart grid," *IEEE Trans. Inf. Forensics Secur.*, vol. 13, no. 8, pp. 2015–2030, Aug. 2018.
- [47] M. N. Kurt, Y. Yılmaz, and X. Wang, "Real-time detection of hybrid and stealthy cyber-attacks in smart grid," *IEEE Trans. Inf. Forensics Secur.*, vol. 14, no. 2, pp. 498–513, Feb. 2019.
- [48] S. Li, Y. Yılmaz, and X. Wang, "Quickest detection of false data injection attack in wide-area smart grids," *IEEE Trans. Smart Grid*, vol. 6, no. 6, pp. 2725–2735, Nov. 2015.
- [49] K. Gajula, V. Le, X. Yao, S. Zou, and L. Herrera, "Quickest detection of series are faults on DC microgrids," in *Proc. IEEE Energy Convers. Congr. Expo.*, 2021, pp. 796–801.
- [50] J. W. Simpson-Porco, F. Dörfler, and F. Bullo, "On resistive networks of constant-power devices," *IEEE Trans. Circuits Syst. II: Exp. Briefs*, vol. 62, no. 8, pp. 811–815, Aug. 2015.
- [51] P. Wheeler and S. Bozhko, "The more electric aircraft: Technology and challenges," *IEEE Electrific. Mag.*, vol. 2, no. 4, pp. 6–12, Dec. 2014.
 [52] P. Wheeler, "Technology for the more and all electric aircraft of the future,"
- [52] P. Wheeler, "Technology for the more and all electric aircraft of the future," in *Proc. IEEE Int. Conf. Automatica*, 2016, pp. 1–5.
- [53] V. Madonna, P. Giangrande, and M. Galea, "Electrical power generation in aircraft: Review, challenges, and opportunities," *IEEE Trans. Transport. Electrific.*, vol. 4, no. 3, pp. 646–659, Sep. 2018.

- [54] R. Abdel-Fadil, A. Eid, and M. Abdel-Salam, "Electrical distribution power systems of modern civil aircrafts," in Proc. 2nd Int. Conf. Energy Syst. Technol., 2013, pp. 201-210.
- [55] P. Midya and P. T. Krein, "Noise properties of pulse-width modulated power converters: Open-loop effects," IEEE Trans. Power Electron., vol. 15, no. 6, pp. 1134-1143, Nov. 2000.
- [56] A. Sangswang and C. O. Nwankpa, "Noise characteristics of DC-DC boost converters: Experimental validation and performance evaluation," IEEE Trans. Ind. Electron., vol. 51, no. 6, pp. 1297–1304, Dec. 2004.
 [57] A. Sangswang and C. Nwankpa, "Random noise in switching DC-DC
- converter: Verification and analysis," in Proc. Int. Symp. Circuits Syst., 2003, pp. III–III.
- B. Zhang and S. Wang, "A survey of EMI research in power electronics systems with wide-bandgap semiconductor devices," IEEE Trans. Emerg. Sel. Topics Power Electron., vol. 8, no. 1, pp. 626–643, Mar. 2020.
- [59] C. M. Bishop and N. M. Nasrabadi, Pattern Recognition and Machine Learning, vol. 4. Berlin, Germany: Springer, 2006.
- [60] F. M. Uriarte et al., "A DC arc model for series faults in low voltage micro-
- grids," *IEEE Trans. Smart Grid*, vol. 3, no. 4, pp. 2063–2070, Dec. 2012. [61] X. Yao, L. Herrera, and J. Wang, "Impact evaluation of series DC arc faults in DC microgrids," in Proc. IEEE Appl. Power Electron. Conf. Expo., 2015, pp. 2953-2958.
- [62] J. Unnikrishnan, V. V. Veeravalli, and S. P. Meyn, "Minimax robust quickest change detection," IEEE Trans. Inf. Theory, vol. 57, no. 3, pp. 1604-1614, Mar. 2011.
- [63] M. Pollak, "Optimal detection of a change in distribution," Ann. Statist., vol. 13, no. 1, pp. 206-227, 1985.
- [64] Photovoltaic (PV) DC Arc-Fault Circuit Protection, Standard 1699B, Underwriters laboratories (UL), Northbrook, IL, USA, 1st ed., 2018.
- "Arc fault circuit interrupter (AFCI) for PV systems," Huawei Technologies Co., Ltd., Technical White Paper, 2020. [Online]. https://solar.huawei.com/en-GB/download?p=%2F-%2Fmedia%2FSolar%2Fnews%2Fwhitepaper%2FAFCI-whitepaper.pdf
- [66] J. Chen, I. A. Kanj, and W. Jia, "Vertex cover: Further observations and further improvements," J. Algorithms, vol. 41, no. 2, pp. 280–301, 2001.
- [67] T. Banerjee and V. V. Veeravalli, "Data-efficient quickest change detection in minimax settings," IEEE Trans. Inf. Theory, vol. 59, no. 10, pp. 6917-6931, Oct. 2013.
- [68] F. Dorfler and F. Bullo, "Kron reduction of graphs with applications to electrical networks," IEEE Trans. Circuits Syst. I: Reg. Papers, vol. 60, no. 1, pp. 150-163, Jan. 2013.
- [69] J. M. Guerrero, J. C. Vasquez, J. Matas, L. G. De Vicuña, and M. Castilla, "Hierarchical control of droop-controlled AC and DC microgrids-A general approach toward standardization," IEEE Trans. Ind. Electron., vol. 58, no. 1, pp. 158-172, Jan. 2011.
- [70] A. Emadi, A. Khaligh, C. Rivetta, and G. Williamson, "Constant power loads and negative impedance instability in automotive systems: Definition, modeling, stability, and control of power electronic converters and motor drives," IEEE Trans. Veh. Technol., vol. 55, no. 4, pp. 1112-1125, Jul. 2006.
- [71] D. Marx, P. Magne, B. Nahid-Mobarakeh, S. Pierfederici, and B. Davat, "Large signal stability analysis tools in DC power systems with constant power loads and variable power loads-A review," IEEE Trans. Power Electron., vol. 27, no. 4, pp. 1773–1787, Apr. 2012.
- [72] A. Bokhari et al., "Experimental determination of the ZIP coefficients for modern residential, commercial, and industrial loads," IEEE Trans. Power Del., vol. 29, no. 3, pp. 1372-1381, Jun. 2014.
- [73] M. P. Supplies, "MagnaDC," 2021. Accessed: Nov. 1, 2021. [Online]. Available: https://magna-power.com/products/magnadc/ts
- [74] S. I. M. Stack, "Semiteachb6u-e1cif-b6ci," 2021. Accessed: Nov. 1, 2021. [Online]. Available: https://shop.semikron-danfoss.com/en/ stacks/semiteach/semiteach-b6u-e1cif-b6ci.html



Kaushik Gajula (Member, IEEE) received the B.E. degree in electronics and communication engineering from SRM University, Chennai, India, in 2016, the M.S. degree in electrical engineering (EE) from the Rochester Institute of Technology, Rochester, NY, USA, in 2018, and the Ph.D. degree in EE from University at Buffalo, Amherst, NY, USA, in 2022.

He is currently a Power Electronics Controls Specialist with Sonnen Inc. His research interests include modeling, control, and optimization of dc microgrids, fault detection using time domain and time-frequency

domain approaches, and control hardware in the loop validation.



Vu Le (Member, IEEE) received the B.S., M.S., and Ph.D. degrees in electrical engineering from the State University of New York at Buffalo, Amherst, NY, USA, in 2016, 2018, and 2021, respectively.

From 2022 to 2023, he was a Research Engineer with the Advanced Power Components Group, University of Dayton Research Institute, Dayton, OH, USA. He is currently a System Engineer with Sierra Nevada Corporation, Sparks, NV, USA. His research interests include dc series arc fault detection, machine learning, and zonal protection.



Xiu Yao (Senior Member, IEEE) received the B.Sc. and M.Sc. degrees from Xi'an Jiaotong University, Xi'an, China, in 2007 and 2010, respectively, and the Ph.D. degree from The Ohio State University, Columbus, OH, USA, in 2015, all in electrical engineering.

She is currently an Associate Professor with the Department of Electrical Engineering, University at Buffalo, Amherst, NY, USA. Her research interests include dc arc detection, dc microgrid protection and control, and high-voltage dc transmission.



Shaofeng Zou (Member, IEEE) received the B.E. degree (with honors) from Shanghai Jiao Tong University, Shanghai, China, in 2011, and the Ph.D. degree in electrical and computer engineering from Syracuse University, Syracuse, NY, USA, in 2016.

He is an Assistant Professor with the Department of Electrical Engineering, University at Buffalo, the State University of New York, Amherst, NY, USA. He was a Postdoctoral Research Associate with the Coordinated Science Lab, University of Illinois at Urbana-Champaign during 2016-2018. His research

interests include reinforcement learning, machine learning, statistical signal processing, and information theory.

Dr. Zou was the recipient of the National Science Foundation CRII award in 2019 and the 2023 AAAI Distinguished Paper Award.



Luis Herrera (Member, IEEE) received the Ph.D. degree in electrical engineering with a focus in power electronics and control from The Ohio State University, Columbus, OH, USA, in 2015.

He is an Assistant Professor with the Department of Electrical Engineering, University at Buffalo, Amherst, NY, USA. From 2016 to 2018, he was an Assistant Professor with the Rochester Institute of Technology. Previously, he was a Research Engineer with the University of Dayton Research Institute working in Intelligent Power Systems sponsored by

the Air Force Research Laboratory, Dayton, OH, USA. His research interests include modeling and control of power electronics, dc microgrids, fault detection using estimation techniques, and power systems optimization.